

The Molecular Disk in the Cloverleaf Quasar

S. Venturini

*Dept. of Physics & Astronomy, State University of New York, Stony Brook,
NY 11794-3800*

Stefano.Venturini@sunysb.edu

P. M. Solomon

Astronomy Program, State University of New York, Stony Brook, NY 11794

PSOLOMON@sbastk.ess.sunysb.edu

ABSTRACT

We propose a new interpretation for the CO emitting region of the Cloverleaf (H1413+1143), a gravitationally lensed QSO. We fit a two-galaxy lensing model directly to the IRAM CO(7-6) data rather than to the optical HST image and from the fit we infer that the CO(7-6) source is a disk-like structure with a characteristic radius of 785 pc¹, a size similar to that of the CO emitting regions present in nearby starburst ultraluminous infrared galaxies. We therefore suggest that the Cloverleaf contains both an extended rotating molecular starburst disk and a central quasar.

Subject headings: Gravitational lensing — quasars: individual (H1413+1143, Cloverleaf) — radio lines:galaxies

1. Introduction

H1413+1143, also known as the Cloverleaf, is a broad absorption line QSO at a redshift of $z = 2.55$ found by Hazard et al. (1984). It was subsequently identified as a lensed object with four bright image components (labeled from A to D as in Figure 1a) by Magain et al. (1988).

¹In the currently widely accepted cosmology: cosmological constant $\Omega_\Lambda = 0.7$, matter content $\Omega_m = 0.3$, and Hubble constant $H_0 = 65 \text{ km s}^{-1} \text{ mpc}^{-1}$.

The earliest indication that molecular emission lines could be present in the Cloverleaf spectrum came from the strong submillimeter dust continuum detected by Barvainis, Antonucci & Coleman (1992) using the James Clerk Maxwell Telescope. Indeed, Barvainis et al. (1994) found CO(3-2) line emission using the Institut de Radioastronomie Millimétrique (IRAM) interferometer. This detection was soon followed by the detection of multiple CO transition lines by Barvainis et al. (1997) using the IRAM 30 m telescope and interferometer. Meanwhile, Wilner, Zhao & Ho (1995) obtained an interferometric map of the CO(3-2) emission using the Berkeley-Illinois-Maryland Array, but with too low spatial resolution to resolve the CO gas structure. Using the Owens Valley Millimeter Array (OVRO), Yun et al. (1997) obtained the first interferometric map of the Cloverleaf in which the CO(7-6) emission was partially resolved. Alloin et al. (1997) obtained a second map with sub-arcsecond resolution of the CO(7-6) line using the IRAM interferometer and Kneib et al. (1998a) further enhanced it with additional data. The enhanced CO(7-6) map fully resolves the four different components of the Cloverleaf.

Kayser et al. (1990) formulated the first lensing models. They described the lensing mass distribution of the two proposed models using respectively a singular isothermal elliptical galaxy and two singular isothermal spherical galaxies of equal masses. They constrained the models using an optical image and added radio features to the lensed source to model the Very Large Array images taken at the National Radio Astronomy Observatory. The resulting fit also suggested the hypothesis that microlensing effects might be present and important. Using these models, Alloin et al. (1997) estimated an upper bound of 1190 pc for the characteristic radius of the CO(7-6) source.

Yun et al. (1997) modeled the lens using an elliptical potential with an external shear and used Hubble Space Telescope (HST) images to constrain the resulting lensing geometry. They constrained the size of the CO(7-6) source using the OVRO CO(7-6) data and estimated the corresponding characteristic radius to be 1420 pc. They also found that the magnification ratios of Keck K-band images reproduced the HST magnification ratios and interpreted this fact as an indication that microlensing was unimportant. However, Østensen et al. (1997) found evidence that the D component of the lensed image is affected by microlensing.

Kneib et al. (1998a) also used the HST images to constrain the lensing geometry. They described the two proposed lensing mass distributions respectively by two truncated elliptical mass distributions (galaxy + dark halo) and a truncated elliptical mass distribution with an external shear (galaxy + cluster). They then used the enhanced IRAM interferometric CO(7-6) map to constrain the size of the CO(7-6) source and estimated the characteristic radii to be respectively 300 pc and 100 pc.

In a subsequent observation, Kneib, Alloin & Pelló (1998b) detected a possible candidate

for the lensing galaxy on HST images. Chae & Turnshek (1999) used the HST images and the position of the detected galaxy to constrain the lensing geometry. They modeled the lensing galaxy mass distribution using elliptical generalized power-law distributions. The proposed models used one single galaxy, one galaxy with external shear, and two galaxies as lenses. The two galaxies model gave the best fit and also the highest microlensing probability to the D component. Chae et al. (2001) observed polarization and intensity variations on HST optical images and suggested that microlensing effects are indeed present on the D component of the lensed image.

Unlike previous estimates of the size of the CO(7-6) source, we model both the source and the lens to obtain a best fit to the IRAM CO(7-6) image. We are thus able to derive an intrinsic size for the CO source using only CO data. Our best fit is able to reproduce the CO(7-6) map geometry as well as the brightness of the four image components. We find that the CO(7-6) source has a characteristic radius of 785 pc, similar to the size of nuclear disks present in local ultraluminous infrared galaxies (ULIRGs²). We therefore suggest that the Cloverleaf has a rotating molecular disk that harbors an extended starburst region, as is the case for nearby ULIRGs, and a central quasar.

This paper is organized in the following way: Section 2 describes the data we use, the model and the fitting procedures adopted, Section 3 presents our main results and comparisons with other models. Section 4 provides discussion, and in Section 5 we state our concluding remarks.

2. The Model

In our fitting procedure we use the velocity-integrated version of the IRAM CO(7-6) map that has been kindly provided to us by R. Barvainis. We make two main assumptions in modeling the IRAM CO(7-6) data. First, we make the assumption that extinction along the line of sight is negligible. Second, we assume that microlensing is negligible in determining the overall geometry of the lensing system. These two assumptions together allow us to compare the map produced by our model to the IRAM CO(7-6) map.

²ULIRGs have by definition high 8–1000 μm luminosities, i.e. $L_{\text{IR}}[8-1000 \mu\text{m}] \geq 10^{12}L_{\odot}$.

2.1. The Cosmology

Angular-diameter distances, which relate angular separations to linear scales in the object frame, are one of the key quantities that enter the lens equation (Schneider, Ehlers & Falco 1992):

$$\boldsymbol{\eta} = \frac{D_s}{D_l} \boldsymbol{\zeta} - D_{sl} \boldsymbol{\alpha}(\boldsymbol{\zeta}), \quad (1)$$

where $\boldsymbol{\eta}$ is the position vector of the QSO in the source plane and $\boldsymbol{\zeta}$ the impact vector of the emitted light ray on the lens plane, $\boldsymbol{\alpha}$ being the deflection angle. D_l and D_s are respectively the angular-diameter distances of the lens and the source from the observer, while D_{sl} is the angular-diameter distance of the source from the lens (see Figure 2). These distances are computed by integrating a Dyer-Roeder differential equation (Dyer & Roeder 1973) for the appropriate cosmology. For the cosmology we use ($\Omega_\Lambda = 0.7$, $\Omega_m = 0.3$), the equation is (Kantowski & Thomas 2001):

$$(1+z) (\Omega_m(1+z)^3 + \Omega_\Lambda) \frac{d^2 D}{dz^2} + \left(\frac{7}{2} \Omega_m(1+z)^3 + 2\Omega_\Lambda \right) \frac{dD}{dz} + \frac{3}{2} \alpha \Omega_m (1+z)^2 D = 0, \quad (2)$$

where D is the angular-diameter distance and $\alpha \in [0, 1]$ is the so-called smoothness parameter. We do not estimate α but we analyze subsequently its impact on the source linear dimensions (see below). For an observer at z_1 and an object at z_2 , the differential equation has the following boundary conditions:

$$\begin{aligned} D(z_1) &= 0 \\ \frac{dD}{dz}(z_1) &= \frac{c}{H_0} \frac{\text{sign}(z_2 - z_1)}{(1+z_1) \sqrt{\Omega_m(1+z_1)^3 + \Omega_\Lambda}}, \end{aligned} \quad (3)$$

where $D(z)$ is the angular-diameter distance of an object at redshift z seen by the observer at redshift z_1 .

2.2. The Lens

The model assumes the presence of two lensing galaxies at a redshift of $z = 1.55$. Each galaxy is modeled as an elliptical generalized power-law mass distribution. The resulting potential responsible of the lensing can be computed using the equations derived in Chae, Khersonsky & Turnshek (1998). The redshift of the lensing object candidate found by Kneib et al. (1998b) is not known and the assumed value of $z = 1.55$ is consistent with the redshift

of observed absorbers in the line of sight (Magain et al. 1988; Turnshek et al. 1988). The angular-diameter distances to the lens and from the lens to the QSO depend on the redshift of the lensing object as seen previously but, since these distances affect only the linear size of the lensing galaxy and the critical density of the lens, the inferred properties of the CO source are not affected by the assumption made.

The elliptical generalized power-law mass distribution takes the following form (Chae et al. 1998):

$$k(\mathbf{x}) = k(r, \phi) = k_0 \left\{ 1 + \left(\frac{r}{r_0} \right)^2 [1 + e \cos 2(\phi - \phi_0)] \right\}^{-\mu-1}, \quad (4)$$

where k_0 is the mass surface density at $r = 0$ (i.e. the center of the distribution) in units of the critical mass density (defined as $c^2 D_s / 4\pi G D_l D_{sl}$), e is the eccentricity, ϕ_0 is the standard position angle, r_0 is the core radius and μ the radial index ($\mu = -1/2$ for an isothermal distribution). To these 5 free parameters, we have to add 2 more which describe the position of the center of the distribution on the lens plane. The total number of free parameters that describe the two galaxies distribution is therefore 14. The only parameter that we do not minimize is the core radius. We arbitrarily keep it at a fixed value of 1.76×10^{-4} arcsec. (1.7 pc at the redshift of $z = 1.55$) for both galaxies, a value similar to the one in Chae & Turnshek (1999). This is primarily due to the behavior of the mass density distribution for rays that are far from the core:

$$k(r, \phi) \approx k_0 r_0^{2\mu+2} \{r^2 [1 + e \cos 2(\phi - \phi_0)]\}^{-\mu-1}. \quad (5)$$

Therefore, a change in the core radius r_0 can be very efficiently compensated by a change in the density k_0 , leading to a flat (actually almost flat) direction in parameter space, an undesirable situation for a minimization routine. The smallness of the value of the core radius is dictated by the need of a rapid convergence in the numerical evaluation of the series expansion of the deflection angle given in Chae et al. (1998).

The source is simply being modeled as a two dimensional Gaussian surface brightness distribution:

$$I(x, y) = I_0 \exp \left\{ -\frac{x^2}{2\sigma_x^2} - \frac{y^2}{2\sigma_y^2} \right\}, \quad (6)$$

where I_0 is the central brightness, $\Delta x = \sqrt{2 \ln 2} \sigma_x$ and $\Delta y = \sqrt{2 \ln 2} \sigma_y$ are the half width at half maximum (HWHM) of the Gaussian while x and y are the coordinates in a coordinate system rotated by a standard position angle ψ_0 . Two more free parameters describe the position of the center of the brightness distribution on the source plane. The total number of free parameters for our model is then 17, having kept the radial index of both galaxies equal.

2.3. The Fitting Procedure

To constrain the parameters of our model, we proceed by minimizing the following $\chi_{d.o.f.}^2$ defined as:

$$\chi_{d.o.f.}^2 = \frac{\sum_{pix} [I_{data}(pix) - I_{model}(pix)]^2 / \sigma^2}{N_{pix} - N_{par}}, \quad (7)$$

where the sum is carried over the pixels of the image. In our case the image is an array of 32×32 pixels, for a total of $N_{pix} = 1024$. N_{par} is an effective number of parameters that also takes into account the fact that image pixels within a beam-width are correlated. It is defined as the number of parameters of the model, i.e. 17, multiplied by the number of pixels per beam-width, 17 in the present case. Therefore we have $N_{par} = 289$. $I_{data}(pix)$ and $I_{mod}(pix)$ are the intensity in the data and in the model maps of corresponding pixels. σ is the noise level of the IRAM CO(7-6) map (Alloin et al. 1997). We determine the values of these 17 parameters by minimizing such $\chi_{d.o.f.}^2$. Due to the large amount of parameters, the choice of a minimization procedure fell on a simulated annealing algorithm such as the one described in Press et al. (1992). As a remark, the number of data points included in the definition of the $\chi_{d.o.f.}^2$ is carefully chosen in order not to make our model over-parametrized but also to have a high signal to noise ratio on the overall image. In order to do so, the original map has been trimmed down to the smallest subset, shown in Figure 1a, containing all the CO(7-6) emission from the Cloverleaf.

3. Results

3.1. Main Results

By fitting our model directly the IRAM CO(7-6) data, we show that it is possible to constrain a lensing geometry even without the use of high resolution optical data such as HST images. Indeed, our model is able to reproduce the geometry as well as the brightness of the four images of the lensed QSO (see Figure 1b). The good agreement with the data is confirmed by the $\chi_{d.o.f.}^2 = 2.8$. This good agreement is also clearly visible from Figure 1c, the difference between data and model. From the same image we also notice that our simple model is not able to account for the weak extended emission. We list in Table 1 the parameters of the fit that describe the lensing galaxies as well as the parameters that describe the source. We notice that the derived position of one of the lensing galaxies is roughly consistent with the position of the candidate lensing galaxy found by Kneib et al. (1998b). We find that the CO(7-6) source has an effective size (HWHM) of $0.0794'' \times 0.0686''$. At the redshift of the Cloverleaf, the angular-diameter distance that relates angular to linear

sizes does not vary more than 26% as α , the smoothness parameter present in the Dyer-Roeder differential equation, ranges from 0 to 1. We fixed its value to 0.5, making less than a 13% error in the linear dimensions of the CO source. With this value of α , the angular size translates into a linear size of 785×678 pc in the adopted cosmology. The source surface brightness peak intensity of 11.8×10^3 K km s⁻¹ corresponds to a gas mass surface density of about 9.5×10^3 M_⊙/pc² if we assume that the conversion factor between CO luminosity (Solomon, Downes & Radford 1992) and gas mass has a value of 0.8 (Downes & Solomon 1998). From our model we find that the CO(7-6) line emission from the QSO is magnified 11 times.

3.2. Comparison with Previous Models

The first model we compare to is Model 1 from Chae & Turnshek (1999). The characteristics of the lenses are rather similar as far as the orientation of the mass isocontours are concerned (33° and 27° compared to 24° and 37°). The eccentricities are somewhat different (0.852 and 0.554 compared to 0.39 and 0.6). The relative position of the two lensing galaxies are also similar, separated by a distance of 0.36 arcseconds instead of 0.5 and with a position angle of 146° instead of 130°. However there is a big difference in the mass distribution since in our model the two galaxies have similar masses while the galaxies in Model 1 have a mass ratio of about 1 : 5.

The subsequent models we consider are from Kneib et al. (1998a). These models differ substantially from our model since we use two galaxies as lens while Kneib et al. (1998a) use a single galaxy, and a galaxy with an external shear. A marked difference occurs in the size of the CO(7-6) source. Our size of 785×678 pc is much larger than the sizes of 300×150 pc and 100×70 pc found by Kneib et al. (1998a). The magnification of 11 that we find is also smaller than the magnification of 18 and 30 found by Kneib et al. (1998a).

The elliptical potential with external shear model by Yun et al. (1997) also differs substantially from our model. The size and magnification of the CO(7-6) source they derive (1420 pc and 10 respectively) are consistent with our estimates. But it is difficult to assess how well their model maps the CO(7-6) images back to a single source on the lens plane since the OVRO CO(7-6) data (as well as its derived blueshifted and redshifted emission images) they base their analysis on is not able to resolve the four components of the Cloverleaf. Moreover, their model is clearly not able to map back all the redshifted CO(7-6) emission to a single source (see Figure 2b in Yun et al. 1997).

Finally we consider the size estimate by Alloin et al. (1997). They derive an upper limit

of 1190 pc for the CO(7-6) source radius, based on the size of the diamond caustic of the single elliptical isothermal galaxy model by Kayser et al. (1990). This estimate is consistent with ours, but it is based on a model that is not able to reproduce the brightness ratio of the different components of the optical image used to constrain it.

4. Discussion: The Molecular Disk

We list the intrinsic properties of the CO(7-6) source in Table 2 where we show the derived CO luminosity. From this table, it is clear that our model accurately accounts for the CO luminosity of the central part of the image containing the four bright image components. If we consider all the CO emission in the image at or above the 4σ level, our model reproduces $\sim 95\%$ of the luminosity. However, the model fails to reproduce the weak extended emission, surrounding the four image components, that contains 22% of the total luminosity.

Given the presence of velocity structure in the IRAM CO(7-6) data and the size estimate from our model, we suggest that the CO(7-6) source might be a rotating disk-like structure with a characteristic radius of 785 pc. Assuming a flat rotation curve, we isolated the part of the Gaussian source that contributes to the redshifted and blueshifted CO(7-6) emission images (see Figure 1c and 1d in Alloin et al. 1997) and produced the corresponding model images. Even with this rough approximation, the model images succeed in reproducing the geometry and the main features of the data images, further confirming our model.

An estimate of the dynamical mass can be made by assuming that the linewidth of the CO(7-6) emission line is due to rotation:

$$M_{dyn} \approx \frac{\Delta V^2 R}{\sin^2(i) G} = \frac{2.6 \times 10^{10}}{\sin^2(i)} M_{\odot} , \quad (8)$$

where ΔV is the half width at zero intensity of 375 km s^{-1} (see Figure 1 in Barvainis et al. 1997), i is the inclination angle from face on and R is the HWHM radius of 785 pc found here. Recalling that for filled disks the CO luminosity traces the geometric mean of the dynamical mass and the gas mass (Downes, Solomon & Radford 1993), we obtain:

$$M_{gas} = \alpha^2 3.0 \times 10^{10} \sin^2(i) M_{\odot} , \quad (9)$$

where α is the conversion factor between M_{gas} and L'_{CO} for virialized clouds. Since the gas mass cannot exceed the dynamical mass, we have: $\alpha \leq 0.9/\sin^2(i)$. For high inclination angles, this value of α becomes similar to the value of about 0.8 found by Downes & Solomon

(1998) for nearby ULIRGs. It becomes comparable to the value of 4.8 found for our Galaxy (Solomon & Barrett 1991) only for unrealistically low inclination angles.

We can also have a rough estimate of the size of the Cloverleaf molecular disk by considering it a black body, made of optically thick dust. We can estimate the temperature of the dust using the 350 μm (roughly 100 μm in the rest frame) and 100 μm (roughly 30 μm in the rest frame) flux ratio:

$$\frac{F_{100} m_{350}}{F_{350} m_{100}} = \frac{\lambda_{350}^3}{\lambda_{100}^3} \frac{\exp(h c (z + 1)/\lambda_{350} k T) - 1}{\exp(h c (z + 1)/\lambda_{100} k T) - 1}, \quad (10)$$

where F_λ (with λ in μm) are the observed fluxes at the observed λ wavelength (see Andreani, Franceschini & Granato 1999, and references therein), m_λ the flux magnification, z the redshift of the Cloverleaf and T the black body temperature. We find that the black body temperature is roughly 135 K, having assumed equal magnification for both fluxes. We estimate a bolometric luminosity of roughly $1.1 \times 10^{14} L_\odot$ from the spectral energy distribution (Granato et al. 1996), assuming an average magnification of 11. This leads to an estimate for the black body size of the dust region:

$$R_{bb} = R_\odot \left(\frac{L}{L_\odot} \right)^{1/2} \left(\frac{T_\odot}{T} \right)^2, \quad (11)$$

where L_\odot , R_\odot , T_\odot are the luminosity, radius and black body temperature of the sun. We find $R_{bb} \simeq 430$ pc. Since the true size must be greater than the optically thick size of 430 pc, the value of 910 pc found by Granato et al. (1996) and our value of 785 pc for the CO(7-6) emitting region are acceptable while the estimates given by Kneib et al. (1998a) of 300 pc and 100 pc for the CO(7-6) emitting region are much too small.

In Table 3 we compare the size and CO luminosity of the source for different cosmologies. The size of the source is similar to the size of nuclear molecular disks present in nearby ULIRGs (Downes & Solomon 1998) as can be seen in Table 4. We would like to stress that we are comparing different lines: the CO(7-6) one of the Cloverleaf and the CO(1-0) one of nearby ULIRGs. It is indeed true that the gas conditions and sizes of the emitting regions that these two lines probe are different. The size of the CO(7-6) emitting region gives a lower bound to the size of the lower excitation CO(1-0) emitting region. It is more difficult though to extend such simple considerations to the brightness temperature, given its complex dependence on the local gas conditions, and therefore to the CO luminosity. Unfortunately, with only the CO(7-6) high resolution interferometric data available, it is not possible to further investigate the observed similarities between these objects.

5. Conclusions

1. *Size of the CO(7-6) emitting region:* The characteristic size (HWHM) of the CO(7-6) line emitting region is 785 pc in the adopted cosmology ($\Omega_\Lambda = 0.7$, $\Omega_m = 0.3$). The size of the lower excitation CO(1-0) line emitting region will be somewhat greater than this. Its size is therefore similar to the size of the nuclear molecular disks present in nearby ULIRGs.
2. *Molecular gas content:* Assuming that the source is indeed a disk-like structure with high inclination and assuming a conversion factor of 0.8 between M_{gas} and L'_{CO} , we find a molecular gas content of about $10^{10} M_\odot$, consistent with the amount of molecular gas found in nearby ULIRGs.
3. *Starburst powered region:* The large size of the CO source (about 1 kpc) seems to rule out a scenario in which the molecular gas is concentrated in a very small region around the central AGN. This is consistent with the molecular gas being heated by a starburst, as in nearby ULIRGs. Therefore, two distinct sources coexist in the Cloverleaf: a central AGN and an extended starburst region.

We would like to thank R. Barvainis for having made the IRAM CO(7-6) integrated map available to us. We would also like to thank A. Evans and J. S. Kim for helpful discussions.

REFERENCES

- Alloin, D., Guilloteau, S., Barvainis, R., Antonucci, R. & Tacconi, L. 1997, A&A, 321, 24
- Andreani, P., Franceschini, A. & Granato, G. 1999, MNRAS, 306, 161
- Barvainis, R., Antonucci, R. & Coleman, P. 1992, ApJ, 399, L19
- Barvainis, R., Tacconi, L., Antonucci, R., Alloin, D. & Coleman, P. 1994, Nature, 371, 586
- Barvainis, R., Maloney, P., Antonucci, R. & Alloin, D. 1997, ApJ, 484, 695B
- Chae, K.-H., Khersonsky, V. K. & Turnshek, D. A. 1998, ApJ, 506, 80
- Chae, K.-H. & Turnshek, D. A. 1999, ApJ, 514, 587
- Chae, K.-H., Turnshek, D. A., Schulte-Ladbeck, R. E., Rao, S. M. & Lupie, O. L. 2001, ApJ, 561, 653

- Downes, D., Solomon, P. M. & Radford, S. J. E 1993, ApJ, 414, L13
- Downes, D. & Solomon, P. M. 1998, ApJ, 507, 615
- Downes, D. & Solomon, P. M. 2003, ApJ, 582, 37
- Dyer, C. C. & Roeder, R. C. 1973, ApJ, 180, L13
- Granato, G. L., Danese, L. & Franceschini, A. 1996, ApJ, 460, L11
- Hazard, C., Morton, D. C., Terlevich, R., & McMahon, R. 1984, ApJ, 282, 33
- Kantowski, R. & Thomas, R. C. 2001, ApJ, 561, 491
- Kayser, R., Surdej, J., Condon, J., Kellerman, K., Magain, P., Remy, M. & Smette, A. 1990, ApJ, 384, 1
- Kneib, J.-P., Alloin, D., Mellier, Y., Guilleaume, S., Barvainis, R. & Antonucci, R. 1998 (a), A&A, 329, 827
- Kneib, J.-P., Alloin, D., & Pelló, R. 1998 (b), A&A, 339, L65
- Lewis, G. F., Carilli C., Papadopoulos, P. & Ivison, R. J. 2002, MNRAS, 330, 15
- Magain, P., Surdej, J., Swings, J.-P., Borgeest, U., Kayser, R., Kuhr, H., Refsdal, S. & Remy, M. 1988, Nature, 334, 325
- Østensen, R., et al. 1997, A&AS, 126, 393
- Press, W. H., Teukolsky, S. A., Vetterling, W. T. & Flannery, B. P. 1992, Numerical Recipes in Fortran, (2d ed.; Cambridge University Press)
- Schneider, P., Ehlers, J. & Falco, E. E. 1992, Gravitational Lenses (1st ed.; Springer)
- Solomon, P. M. & Barrett, J. W. 1991, in “Dynamics of Galaxies and Their Molecular Cloud Distributions”, ed. F. Combes & F. Casoli (Kluwer Academic Publishers), 235
- Solomon, P. M., Downes, D. & Radford, S. J. E. 1992, ApJ, 398, L29
- Turnshek, D. A., Foltz, C. B., Grillmair, C. J. & Weyman, R. J. 1988, ApJ, 325, 651
- Wilner, D. J., Zhao, J.-H. & Ho, P. T. P. 1995, ApJ, 452, L91
- Yun, M., Scoville, N. Z., Carrasco, J. J. & Blandford, R. D. 1997, ApJ, 479, L9

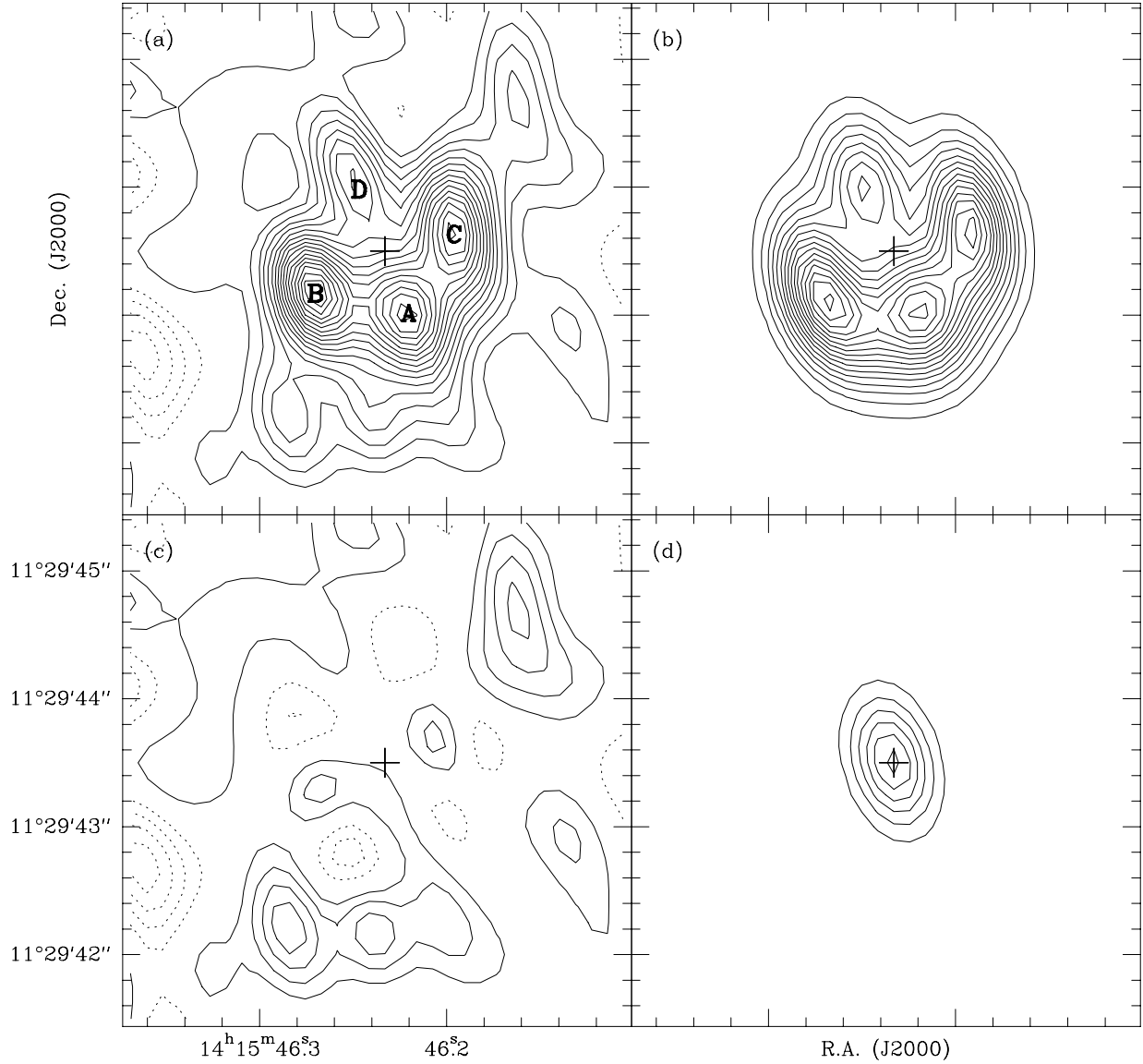


Fig. 1.— (a) Integrated IRAM CO(7-6) map. (b) Model map. (c) Difference between data and model (a–b). (d) Unlensed CO source. In all the figures, the beam is $0.77'' \times 0.44''$ at a P.A. of 15° , with $T_b/S = 70 \text{ K Jy}^{-1}$, and the 1σ contours are $0.55 \text{ Jy km s}^{-1} \text{ beam}^{-1}$.

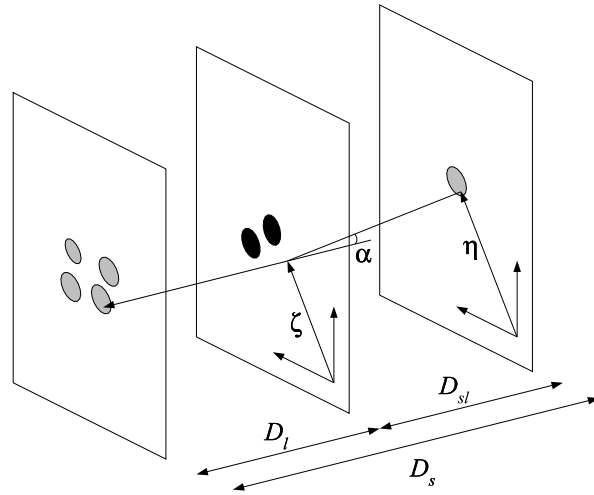


Fig. 2.— A light ray from the source with position vector η on the source plane and impact parameter ζ on the lens plane is deflected by the deflection angle α . Also shown are the angular-diameter distances.

Table 1. Model Parameters ^a

Lens Parameters	
Galaxy 1	
k_0 ($10^6 M_\odot \text{ pc}^{-2}$)	18.3 ± 0.4
e	0.554 ± 0.005
P.A. ^b (deg.)	27.0 ± 0.4
x_G, y_G ^c (10^{-2} arcsec.)	$20.8 \pm 0.3, -14.7 \pm 0.6$
μ ^d	-0.381 ± 0.002
Galaxy 2	
k_0 ($10^6 M_\odot \text{ pc}^{-2}$)	12.7 ± 0.1
e	0.852 ± 0.005
P.A. ^b (deg.)	33.0 ± 0.5
x_G, y_G ^c (10^{-2} arcsec.)	$0.69 \pm 0.07, 15.3 \pm 0.2$
μ ^d	-0.381 ± 0.002
Source Parameters	
I_0 (10^3 K km s^{-1})	11.8 ± 0.2
$\Delta x, \Delta y$ (10^{-2} arcsec.)	$7.94 \pm 0.04, 6.86 \pm 0.04$ ^e
P.A. ^b (deg.)	55 ± 1
x_S, y_S ^c (10^{-2} arcsec.)	$7.56 \pm 0.05, -5.07 \pm 0.05$

^aError is computed as $\chi_{min}^2 + 1.0$.

^bPosition angle is East of North.

^cOffsets are with respect to the center of the IRAM CO(7-6) map at $14^{\text{h}}15^{\text{m}}46^{\text{s}}.233$ RA and $11^\circ29'43''.50$ DEC, 2000 epoch.

^dThe radial index is kept equal for both galaxies.

^eHalf width at half power. In the adopted cosmology the corresponding linear sizes are $(785 \pm 5, 678 \pm 5)$ pc.

Table 2. Source Properties

	L'_{CO} $10^{10} \text{ K km s}^{-1} \text{ pc}^2$	L_{CO} $10^8 L_{\odot}$
Total Luminosity		
Data	40 ± 1	68 ± 3
Model Lensed	31 ± 1	53 ± 2
Model Unlensed	2.8 ± 0.1	4.8 ± 0.2
Central Luminosity ^a		
Data	29 ± 1	49 ± 2
Model Lensed	28 ± 1	47 ± 1

^aWithin the 4σ contour in the IRAM CO(7-6) map, i.e. including the four image components and excluding the weak extended emission.

Table 3. Source Properties in Different Cosmologies

α	L'_{CO} Data 10^{10} K km s $^{-1}$ pc 2	L'_{CO} Model Unlensed 10^{10} K km s $^{-1}$ pc 2	$(\Delta x, \Delta y)^a$ pc
$\Omega_m = 0.3, \Omega_\Lambda = 0.7, H_0 = 65$ km s $^{-1}$ mpc $^{-1}$			
0.0	51	3.6	(891, 770)
0.5	40	2.8	(785, 678)
1.0	30	2.1	(687, 594)
$\Omega_m = 1.0, \Omega_\Lambda = 0.0, H_0 = 75$ km s $^{-1}$ mpc $^{-1}$			
0.0	22	1.6	(590, 509)
0.5	16	1.1	(493, 426)
1.0	11	0.7	(407, 351)

^aHalf width at half power (HWHM).

Table 4. Sizes of CO Emitting Regions in ULIRGs and High z CO Sources

	z	CO Line	Radius ^a pc	True T_b K	L'_{CO} ^b 10^9 K km s ⁻¹ pc ²	Reference
Arp 220	0.02	1 – 0	560	29	7.9	1
Mrk 231	0.04	1 – 0	540	56	7.0	1
Mrk 273	0.04	1 – 0	460	36	7.4	1
VII Zw 31	0.05	1 – 0	1300	18	12.0	1
IRAS 10214+4724 ^c	2.29	3 – 2	540	40	11.0	2
		6 – 5	540	23	6.4	2
Cloverleaf	2.55	7 – 6	785	32	28.0	3
SMM J14011+0252	2.56	3 – 2	410	35	5.7	4
		7 – 6	480	7	1.3	4
APM08279+5255 ^d	3.91	1 – 0	1160	16	35.0	5

^aHalf power radius (HWHM).

^bIntrinsic luminosity.

^cAssuming a magnification of 15.

^dAssuming a magnification of 7.

References. — (1)Downes & Solomon (1998); (2)Solomon et al. (1992); (3)This article; (4)Downes & Solomon (2003); (5)Lewis et al. (2002).